Macromolecules

Article

pubs.acs.org/Macromolecules

# In Depth Analysis on the Unusual Multistep Aggregation Process of Oligo(ethylene glycol) Methacrylate-Based Polymers in Water

Bo Zhang, Hui Tang, and Peiyi Wu*

Stat Key Laboratory of Molecular Engineering of Polymers, Department of Macromolecular Science, and Laboratory of Advanced Materials, Fudan University, Shanghai, 200433, China

Supporting Information

**ABSTRACT:** Dynamic thermal phase transition behavior of a thermoresponsive copolymer P($MEO_2MA$-*co*-$PEGMA_{2080}$) synthesized by ATRP random copolymerization of 2-(2-methoxyethoxy)ethyl methacrylate($MEO_2MA$, $M_n$ = 188 g/mol) and poly(ethylene glycol) methyl ether methacrylate (PEGMA, $M_n$= 2080 g/mol) in $D_2O$ was studied by means of infrared spectroscopy in combination with two-dimensional correlation analysis (2Dcos). Because of the absence of strong intermolecular hydrogen bonding interactions between polymer chains and the amphiphilic property of $PEGMA_{2080}$ with long ethylene glycol segments, this copolymer exhibited an unusual thermally induced multistep aggregation process. In general, the change of hydrophilic side chain takes place before carbonyl groups and backbones during the whole process and thus the driving force of this phase transition process of P($MEO_2MA$-*co*-$PEGMA_{2080}$) should be hydration changes of side chains. 2Dcos was finally employed to discern the sequence order of all the group motions during heating process in different temperature regions. It is concluded that during the phase transition P($MEO_2MA$-*co*-$PEGMA_{2080}$) chains successively experience "unimers−clusters−micelles− aggregates" four consecutive conformation changes.

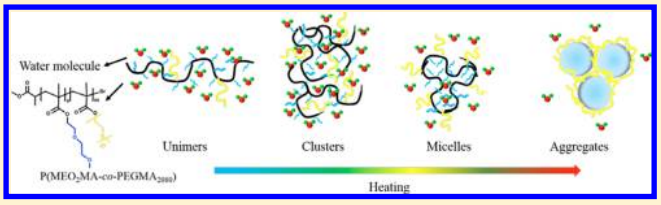


## 1. INTRODUCTION

Thermoresponsive polymers have attracted increasing interests due to their promising potential for the preparation of a wide variety of smart responsive materials such as biosensors, matrices for tissue engineering, and drug delivery carriers.[1−3] Poly(*N*-isopropylacrylamide) (PNIPAM), a prominent temperature-sensitive polymer with lower critical solution temperature(LCST, ∼32 °C) close to physiological temperature, has been widely studied.[4] PNIPAM chains adopt an extended chain conformation below its LCST and undergo an abrupt coil-to-globule phase transition when the temperature goes above its LCST.[5] However, the nonignorable hysteresis, strong hydrogen-bonding interactions with proteins, and toxic low-molecular weight amines produced during hydrolysis would have greatly limited the application of PNIPAM in the biotechnology field.[6] Recently, a new family of polymers based on oligo(ethylene glycol) methacrylate(OEGMA) with thermally responsive properties have been developed.[7−10] POEMGA exhibits fascinating features including good biocompatibility, tunable LCST, antifouling properties at temperatures below their LCST, and complete reversibility of thermal transition without significant hysteresis,[11−13] which endows POEGMA to be widely used in many fields such as polymer brushes, nanohybrid materials, bioactive surfaces, and hydrogels.[13−18]

The tunable LCST of POEMGA could be realized using a simple random copolymerization[10,19−22] of OEGMA with different hydrophilicity but similar chemical nature. By ATRP random copolymerization of 2-(2-methoxyethoxy)ethyl methacrylate ($MEO_2MA$, $n$ = 2) and OEGMA ($n$ = 8−9, $M_n$ = 475 g/mol), Lutz and co-workers prepared a series of thermoresponsive P($MEO_2MA$-*co*-$OEGMA_{475}$) copolymers with LCST varying from 26 to 90 °C by changing comonomer composition.[10] In recent years, many researches have been done to study the thermoresponsive behavior of POEGMA. According to Lutz's study, the polymer would favor interactions with water to allow solubilization at room temperature and undergo a coil-to-globule phase transition when heated to above LCST with mainly hydrophobic polymer−polymer interactions in the system.[7] Our group have also explored the dynamic self-aggregation and self-disaggregation mechanism of thermoresponsive POEGMA chains in water during heating and cooling process and found that the self-aggregation process of P($MEO_2MA$-*co*-$OEGMA_{475}$) is dominated by the conformation changes of side chains.[23] By mixing two POEGMA chains with different molecular weights, Gibson et al. found that two independent phase transitions would be observed due to a weak molecular weight dependence on its cloud point.[24] POEGMA block copolymers also possess similar property, as reported by Tam and co-workers.[25] More interestingly, Peng et al. synthesized a random copolymer P($MEO_2MA$-*co*-$PEGMA_{2080}$) containing $MEO_2MA$ and PEGMA which exhibited an unusual thermally induced two-stage aggregation process.[26] By TEM, light scattering measurements, they

**Received:** April 15, 2014
**Revised:** June 29, 2014
**Published:** July 7, 2014

   dx.doi.org/10.1021/ma500774g | *Macromolecules* 2014, 47, 4728−4737

proposed that, upon increasing the temperature, the copolymer chains would phase separate, associate, and rearrange to produce stable micelles and the morphology of the micelle with a methacrylate core was stabilized by the longer ethylene glycol segment shell. Similar two-stage aggregation have been reported in other various block copolymers comprising two or more thermal-sensitive blocks, where these systems displayed sharp and rapid temperature-induced self-assembly behaviors.[27−31]

However, to the best of our knowledge, no integrated dynamic mechanism of the thermally induced phase transition of P($MEO_2MA$-*co*-$PEGMA_{2080}$) during heating processes has ever been clarified. Herein, in our paper, we attempt to apply IR spectroscopy in combination with two-dimensional correlation spectroscopy (2Dcos) to illustrate the dynamic hydration behavior of P($MEO_2MA$-*co*-$PEGMA_{2080}$) during the heating process. Additional information on the specific order taking place corresponding to chain conformation changes during phase transition could be extracted, which is very helpful for further understanding the evolution mechanism of micelle formation of P($MEO_2MA$-*co*-$PEGMA_{2080}$).

## 2. EXPERIMENTAL SECTION

**2.1. Materials.** 2-(2-Methoxyethoxy)ethyl methacrylate ($MEO_2MA$) ($M_n$= 188g/mol, 95%), poly(ethylene glycol) methyl ether methacrylate (PEGMA) ($M_n$= 2080g/mol, 50 wt % in water) were purchased from Sigma-Aldrich and purified by passing them through a column filled with basic alumina prior to use. Methyl 2-bromopropionate (MBP), copper(I) chloride, 2, 2′-bipyridyl (Bipy), and ethanol were purchased from Aladdin and used as received.

P($MEO_2MA$-*co*-$PEGMA_{2080}$) was synthesized via atom transfer radical copolymerization of $MEO_2MA$ and PEGMA monomers according to literature.[26] A typical procedure is described as follows: a reaction tube was charged with $MEO_2MA$ (2.277 g, 12.1 mmol), PEGMA (2080 g/mol) (0.52 g, 0.125 mmol), CuBr (35.9 mg, 0.25 mmol), Bipy (78.1 mg, 0.5 mmol), methyl 2-bromopropionate (20.9 mg, 0.125 mmol) and ethanol (3.5 mL). After three freeze−pump−thaw cycles, the reaction mixture was sealed under vacuum and the reaction was allowed to continue at 60 °C for 3h, and the reaction was stopped by exposing the flask to liquid nitrogen. The reacted mixture was dialyzed against Millipore water for 3 days, and the final product was collected after freeze-drying.

GPC measurements with monodisperse polystyrene as standard and THF as eluent phase at 35 °C were utilized to determine the number-average molecular weight ($M_n$) and polydispersity index (PDI = $M_w$/$M_n$) of P($MEO_2MA$-*co*-$PEGMA_{2080}$), as shown in Figure S1. The resulting copolymer (chemical structure as shown in Scheme 1) has $M_n$ = 1.90 × $10^4$ g/mol and PDI = 1.35. The $^1$H NMR spectra of P($MEO_2MA$-*co*-$PEGMA_{2080}$) is shown in Figure S2, and all the peaks corresponding to the protons on the copolymer are assigned according to literature.[32] $D_2O$ was purchased from Cambridge Isotope Laboratories Inc. (D-99.9%). The concentration of P($MEO_2MA$-*co*-$PEGMA_{2080}$) in $D_2O$ was fixed to 10 wt % and placed at 4 °C for a week before FT-IR measurements to ensure complete dissolution.

**Scheme 1. Chemical Structure of P($MEO_2MA$-*co*-$PEGMA_{2080}$)**

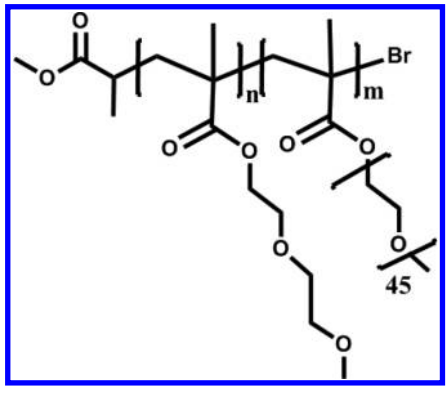


**2.2. Instruments and Measurements.** Turbidity measurements were carried out at 500 nm on a Lamda 35 UV−vis spectrometer with deionized water as reference (100% transmittance). Temperatures were regulated manually with a water-jacketed cell holder at the rate of ca. 0.5 °C/min with an increment of 1 °C. To ensure thermal equilibrium of the sample cell, each temperature point was held for 1 min before measurement. The temperature-dependent average hydrodynamic radius ($R_h$) measurements of P($MEO_2MA$-*co*-$PEGMA_{2080}$) in $H_2O$ (10 wt %) were performed on a dynamic light scattering− (DLS−) zetasizer nanosystem (Malvern) with an increment of 1 °C from 20 to 59 °C.

The sample of P($MEO_2MA$-*co*-$PEGMA_{2080}$) solution for FT-IR measurements was prepared by being sealed between two ZnS tablets. All the time-resolved FTIR spectra at variable temperatures were recorded by using a Nicolet Nexus 6700 FTIR spectrometer equipped with a DTGS detector. 32 scans at a resolution of 4 $cm^{-1}$ were accumulated to obtain an acceptable signal-to-noise ratio. Temperatures were manually controlled with an electronic cell holder at rate of ca. 0.3 °C/min with an increment of 1 °C(accuracy: 0.1 °C). Baseline correction was performed by the software of OMINIC 6.1a.

**2.3. Investigation Methods.** *Two-Dimensional Correlation Analysis (2Dcos).* The temperature-dependent FTIR spectra recorded at an internal of 1 °C in certain wavenumber ranges were selected to perform 2D correlation analysis. 2D correlation analysis was conducted using the software of 2D Shige ver. 1.3 (Shigeaki Morita, Kwansei Gakuin University, Japan, 2004−2005) and was further plotted into the contour maps by Origin Program ver. 8.0. In the contour maps, red colors are defined as positive intensities, while the blue colors are defined as negative ones.

## 3. RESULTS AND DISCUSSION

**3.1. Turbidity and DLS Measurements.** Herein, temperature-dependent UV/vis transmittance measurements at the wavelength of 500 nm of 10 wt % copolymer aqueous solution were performed, as shown in Figure 1. The thermoresponsive properties of the dilute P($MEO_2MA$-*co*-$PEGMA_{2080}$) copolymer aqueous solution with different concentrations have been elaborated in literature.[26] According to their research, the critical phase transition temperatures remained constant and the turbidity curves were similar, implying that the phase transitions of P($MEO_2MA$-*co*-$PEGMA_{2080}$) in water were

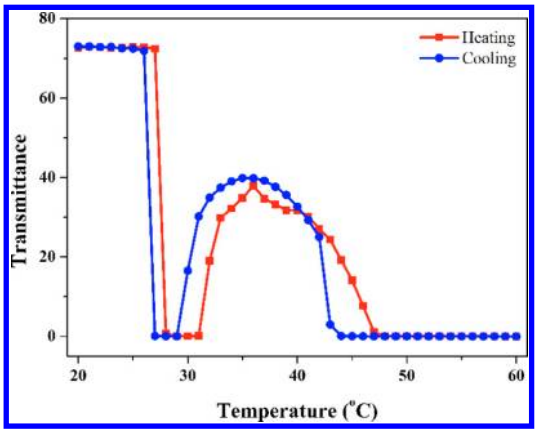


**Figure 1.** Transmittance vs temperature for 10 wt % P($MEO_2MA$-*co*-$PEGMA_{2080}$) aqueous solution at the wavelength of 500 nm. Heating and cooling rates are 0.5 °C/min.


dx.doi.org/10.1021/ma500774g | Macromolecules 2014, 47, 4728−4737

insensitive to polymer concentration. However, in our case (relativly concentrated solution), a slightly different phenomenon could be observed. The optical photographs of 10 wt % P($MEO_2MA$-*co*-$PEGMA_{2080}$) aqueous solution at different temperatures in the heating process is shown in Figure 2, which could well correspond to the transmittance change. Detailed descriptions with transmittance change were in the following discussion.

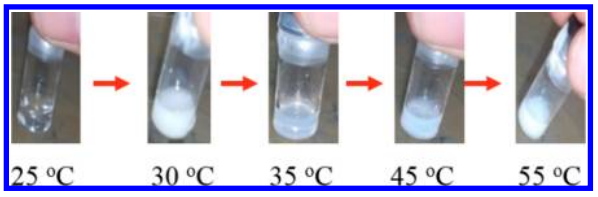


**Figure 2.** Optical photographs of 10 wt % P($MEO_2MA$-*co*-$PEGMA_{2080}$) aqueous solution at different temperatures in a heating process.

The solution was transparent at low temperature, as shown in Figure 2, and the transmittance is ca. 70% due to the relatively high concentration. Upon heating, the solution turned totally cloudy at 28 °C. The color of the solution remains white in the temperature range 28 to 31 °C, corresponding to a zero transmittance (% *T*). According to literature, such behavior is due to the dehydration of polymer backbone consisting of short oligo(ethylene glycol) methacrylates side chains and the polymer chains adopted a compact globular structure induced by the intra- and intermolecular aggregation of the polymeric chains.[26] Additionally, the platform existed from 28 to 31 °C was different from that in Peng et al.'s research, where only one peak around 30 °C could be identified.[26] This could be attributed to the high concentration of the copolymer in our system. When the concentration of P($MEO_2MA$-*co*-$PEGMA_{2080}$) was low, the structure formed at around 30 °C would be easy to change as most polymer chains are independent in solutions. However, in concentrated solution system, the assembly of large number of P($MEO_2MA$-*co*-$PEGMA_{2080}$) would result in fast decrease of transmittance and polymer chains would interact with each other in the collapsed state, thus higher temperature were need to change the conformation of the copolymer. The solution became less turbid when the temperature was further raised to 32 °C. The polymer solution exhibited light blue color in the temperature range between 33 to 41 °C, as shown in Figure 2, and a platform with the transmittance at ca. 30% could be observed. Upon further heating, the polymer solution turned white again and the transmittance decreased to a steady value of 0% when the temperature exceeded 49 °C. The resultant solution status is different from colloidal status, which has been reported in previous literature.[26] In Liu's research, the final state of the copolymer was a stable core−shell micellar structure stabilized by $PEGMA_{2080}$ with low concentration. The difference could be attributed to high polymer concentration. In our research, the polymer concentration was much higher (~10 wt %). Polymer chains were densely packed and interacted with each other to form aggregates in the whole system, which resulted in the 0% transmittance. Upon cooling, the apparent phenomenon and the transmittance change is almost converse to the heating process with some hysteresis. Additionally, the platform around 33 to 41 °C was more gentle compared to the heating process, which could be possibly due to the formation of dense homogeneous structure in high temperature.

The hydrodynamic radii ($R_h$) as a function of temperature of 10 wt % P($MEO_2MA$-*co*-$PEGMA_{2080}$) in aqueous solution determined from DLS measurements at various scattering angles are shown in Figure 3. At low temperature, the $R_h$ values

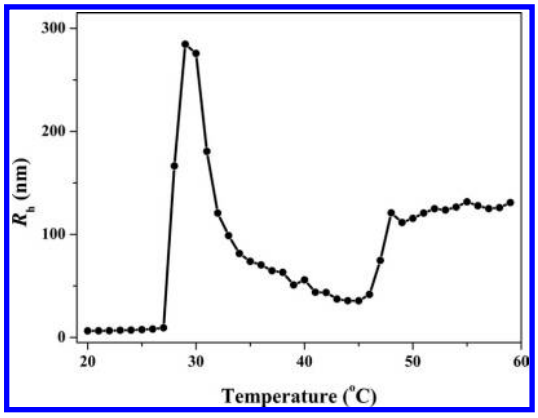


**Figure 3.** $R_h$ of 10 wt % P($MEO_2MA$-*co*-$PEGMA_{2080}$) aqueous solution at different temperatures in a heating process.

were small (~6 nm), indicating the presence of single polymeric chains. The $R_h$ values suddenly increased at 28 °C and reached 284 nm at 29 °C, suggesting the formation of large clusters, which are in good agreement with the minima in the transmittance plot and optical photographs (Figures 1 and 2). On further heating to 33 °C, the particle size greatly decreased and remained relatively constant at around 50 nm, which could well correspond to the platform in the temperature range between 33 to 41 °C in Figure 1. During this temperature range, a core−shell micellar structure was formed,[26] which could correspond to the light blue solution in Figure 2. As large clusters separated to form small micelle, the solution became less turbid in this temperature region, as shown in Figure 1. Upon further heating, the $R_h$ values increased and remained relatively constant at around 100 nm, implying the formation of dense aggregates, which are in good agreement with the second minima in the transmittance plot.

**3.2. Conventional IR Analysis.** Temperature-dependent FT-IR measurements of P($MEO_2MA$-*co*-$PEGMA_{2080}$) in $D_2O$ (10 wt %) were performed during a heating process between 20 and 59 °C to elucidate the dynamic mechanism of the thermoresponsive behavior, as shown in Figure 4. It should be noted that we used $D_2O$, instead of $H_2O$, as the solvent R to eliminate the overlap of $\delta$(O−H) band of $H_2O$ around 1640 $cm^{-1}$ with $\nu$(C═O) of P($MEO_2MA$-*co*-$PEGMA_{2080}$) as well as the broad $\nu$(O−H) band of $H_2O$ around 3300 $cm^{-1}$ with $\nu$(C−H) bands.[23] As is known, the deuterium isotope effect would not result in obvious changes on the phase transition behavior of OEGMA-based polymer.[23]

Herein, we specifically focus on the following three spectral regions: C−H stretching region (3020−2810 $cm^{-1}$), C═O stretching region (1750−1680 $cm^{-1}$), and C−O−C stretching region (1120−1070 $cm^{-1}$). In this way, we are able to trace almost all the group motions of P($MEO_2MA$-*co*-$PEGMA_{2080}$) during the phase transition. As shown in Figure 4, during the heating process, all the C−H stretching bands shift to lower frequency, indicating the gradual dehydration of P($MEO_2MA$-*co*-$PEGMA_{2080}$) backbones and side chains. As is known, water clathrates exist around the hydrophobic moieties of water-


dx.doi.org/10.1021/ma500774g | Macromolecules 2014, 47, 4728−4737

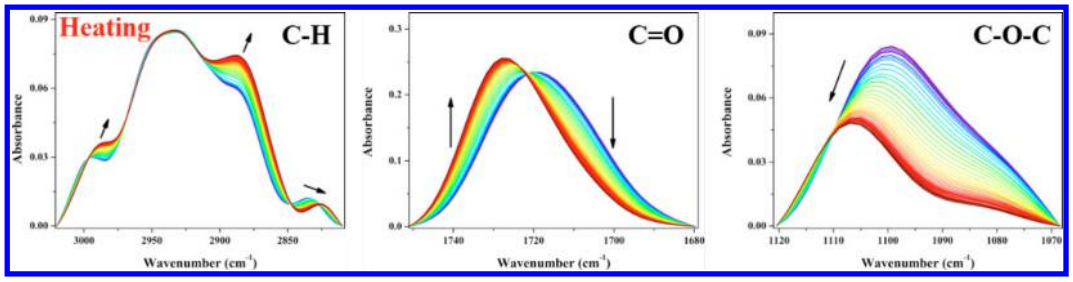


**Figure 4.** Temperature-dependent FTIR spectra of P($MEO_2MA$-*co*-$PEGMA_{2080}$) in $D_2O$ (10 wt %) during heating between 20 and 59 °C with an interval of 1 °C in the regions 3020−2810, 1750−1680, 1120−1070 $cm^{-1}$.

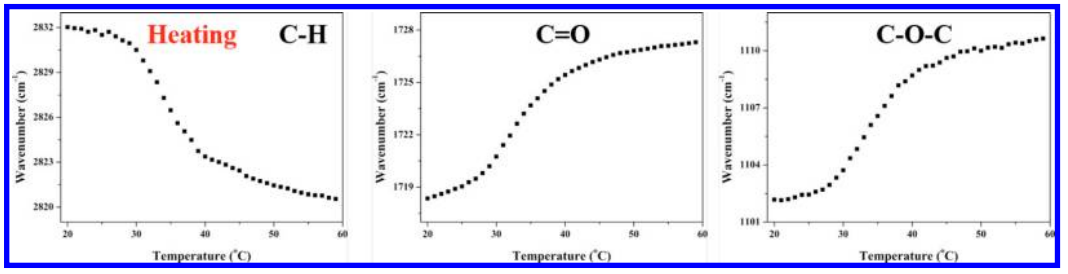


**Figure 5.** Temperature-dependent frequency shifts of $\nu_s(CH_2)(-OCH_2CH_2O-)$, $\nu$ (C═O), and $\nu$(C−O−C)during heating between 20 and 59 °C with an interval of 1 °C, respectively.

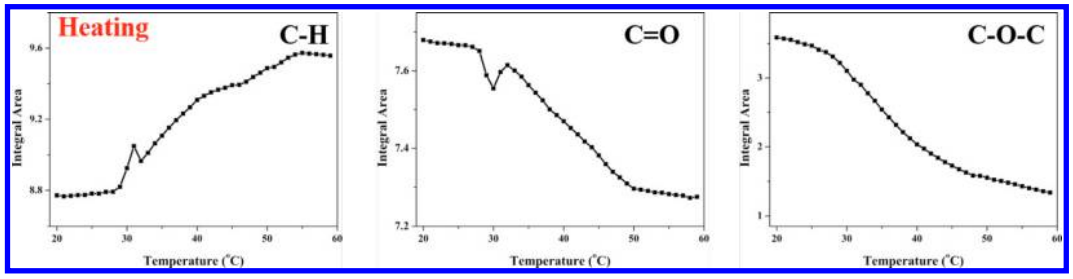


**Figure 6.** Temperature-dependent integral area of $\nu_s(CH_2)(-OCH_2CH_2O-)$, $\nu$(C═O), and $\nu$(C−O−C)during heating between 20 and 59 °C with an interval of 1 °C, respectively.

soluble polymers in a well-ordered structure and more water molecules surrounding C−H groups would result in higher vibrational frequency.[33,34] Meanwhile, the main bands corresponding to C═O and C−O−C exhibit a blue shift, suggesting the dehydration of hydrophobic ester linkages and the abruption of hydrogen bonds between ether oxygen groups and water. Thus, together with the increase in hydrophobicity of the polymer chains, water molecules are expelled out of the polymer chains, as can be identified in the temperature-resolved FTIR spectra.

To characterize the more detailed information on temperature's influence on the hydration states of different chemical groups during the phase transition of P ($MEO_2MA$-*co*-$PEGMA_{2080}$), we additionally examine the temperature-dependent frequency shifts of the bands around 2832, 1720, and 1102 $cm^{-1}$ corresponding to $\nu_s(CH_2)(-OCH_2CH_2O-)$, $\nu$(C═O), and $\nu$(C−O−C), whose peak positions can be easily determined, as shown in Figure 5.

The integral area of $\nu_s(CH_2)(-OCH_2CH_2O-)$, $\nu$(C═O), and $\nu$(C−O−C) during heating have been shown in Figure 6. During heating, the integral area of C═O sharply decreased at 28 °C and reached a lower point at around 30 °C. With further heating, a reverse trend could be detected, with the integral area raised to a higher point at around 32 °C. The integral area gradually decreases to a relatively stable value in the following process, implying the completion of the phase transition. In general, the changing trend of the integral area of C═O is similar to turbidity results, which could be summarized as a two-stage aggregation. Similar trend with the opposite direction could be observed in the integral area change of CH, implying the cooperativity of different part of the polymer. The opposite changing direction between C═O and CH could be attributed to the different interactions with water, which could also be found in the changing difference in frequency shifts. However, no similar trend could be detected in the integral area change of C−O−C, while the change is similar to that of frequency shifting tendency, as discussed before. However, as far as we are concerned, the difference between CH, C═O, and C−O−C should be attributed to the different locations of different groups on the polymer chain. As CH regions contains both the CH in backbone and side chain and C═O are located in the binding site of backbone and side chain, the integral area change of these two functional groups could represent the overall changes of the whole polymer chain. As a result, the integral area change of these two functional groups are in good accordance with the turbidity results. However, C−O−C group is only located in the flexible hydrophilic side chain, the phase transition process is relatively independent compared to the whole polymer chain, which could account for the integral area change of C−O−C in the heating process.

C═O group, as a representative group of the polymer chain, was selected for further analysis. The $\nu$(C═O) is fitted with


dx.doi.org/10.1021/ma500774g | *Macromolecules* 2014, 47, 4728−4737

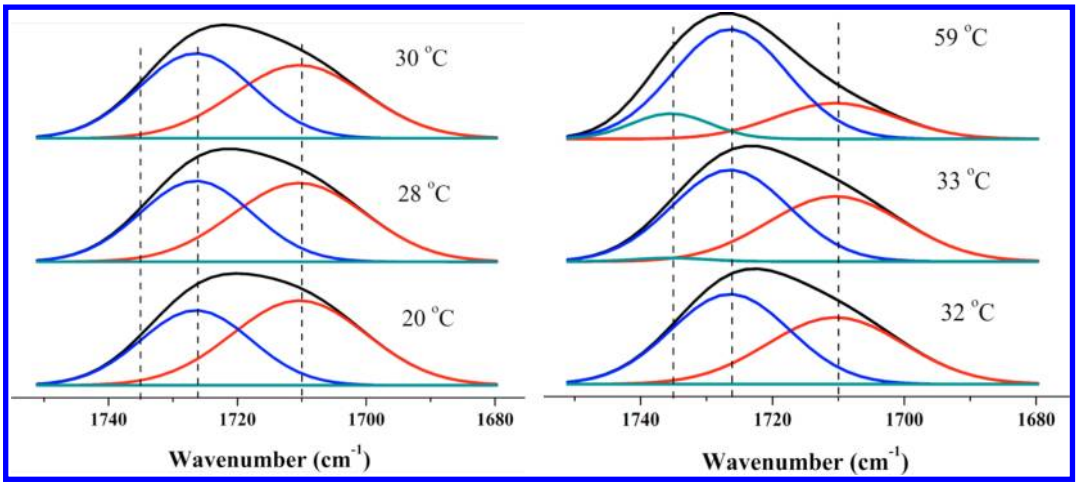


**Figure 7.** Baseline-corrected $\nu$ (C═O) bands measured during the heating process. The color lines indicate the Gaussian fit to separate different components.

Gaussian curves with three bands located at 1735, 1726, and 1710 $cm^{-1}$, as shown in Figure 7. The three bands are based on the results of detailed 2D analysis in different heating process, as discussed below. It is well-known that $\nu$(C═O) shifts toward lower wavenumbers when the carbonyl group is hydrogen bonded. The 1735 $cm^{-1}$ band was assigned to dehydrated C═O. The band at 1710 $cm^{-1}$ could be assigned to H-bonded carbonyl groups with water molecules, which should be simply called as the hydrated C═O.[23] The band at 1726 $cm^{-1}$, was defined as semidehydrated C═O, which represented two or more carbonyl groups H-bonded with one water molecule. The band at 1726 $cm^{-1}$ represented a relative hydrophobic state, which existed between dehydrated C═O and hydrated C═O.

Here, spectra at six different temperatures during the heating process are chosen as examples. Curve fitting reveals that two or three bands are necessary to match the spectra at different temperatures satisfactorily. It should be pointed out that the area experiences an obvious variation during heating process, as discussed before. The integral area underwent a two-step decreasing transition with a reverse transition state. The complex change contains an apparent decrease in the absorbance of the lower frequency components and an apparent increase of the higher frequency. As is known to all, the area reflects the relative content of the groups. The integral area is equal to absorbance in a sense, and the absorbance can be described according to the Beer−Lambert law:

$$I_i = a_i bc$$

where $a_i$ is the absorption coefficient, $b$ is the path length, and $c$ represents the concentration of the species. In our research, the absolute value of $b$ is unknown but it is constant through the investigations. Absorbance changes of three components belong to the $\nu$(C═O) band during the heating process are shown in Figure 8. In general, the area of both 1726 and 1735 $cm^{-1}$ bands increase while the area of the 1710 $cm^{-1}$ band decrease during the heating process. As the total area decreases finally, one can deduce that the area increment of 1726 and 1735 $cm^{-1}$ cannot make up the decrement which corresponds to 1710 $cm^{-1}$. According to previous study, the absorption coefficient $a_i$ strong depended on the frequency.[35] The three components here at different frequency will have different $a_i$. In this way, the total area decrement is owing to a smaller ai of 1726 and 1735 $cm^{-1}$ than 1710 $cm^{-1}$.

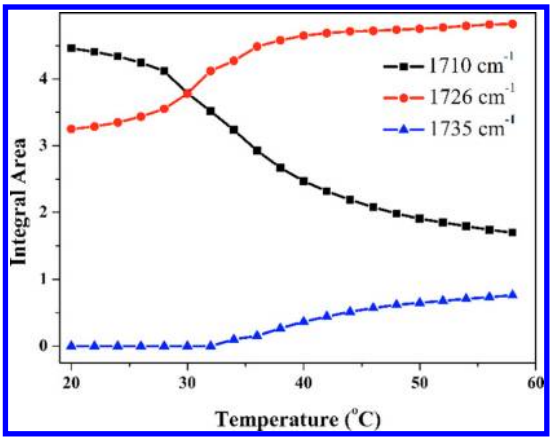


**Figure 8.** Integral area of bands at 1710, 1726, and 1735 $cm^{-1}$ vs temperature during the heating process.

However, quantitative analysis of relative content or fraction of each component seem to be difficult because of the complicated changes during temperature variations. Figure 8 presents a quantitative analysis of each component's area variation versus temperature. In detail, the integral area of the band at 1735 $cm^{-1}$ remained 0 until 32 °C in the heating process. The phase transition between 20 and 32 °C could be roughly identified as the transition between 1710 and 1726 $cm^{-1}$attributed to hydrated C═O and semidehydrated C═O, respectively. The structure formed at 30 °C was not a dense hydrophobic structure because no dehydrated C═O bands could be detected. Thus, the loose structure provided a possible chance for further structural adjustment to form a micelle structure at 32 °C. The band at 1735 $cm^{-1}$ began to emerge at 33 °C, implying the beginning of formation of dense hydrophobic structure. In the following heating process, the integral area of the band at 1735 and 1726 $cm^{-1}$ increased with the decreasing of that of the band at 1710 $cm^{-1}$. In the resultant structure, the semidehydrated and dehydrated C═O occupied the mainly part of the whole C═O peak, implying the formation of a dense hydrophobic structure. However, the results obtained from curve fitting could only provide limited information and more detailed discussion are in the following part.


dx.doi.org/10.1021/ma500774g | Macromolecules 2014, 47, 4728−4737

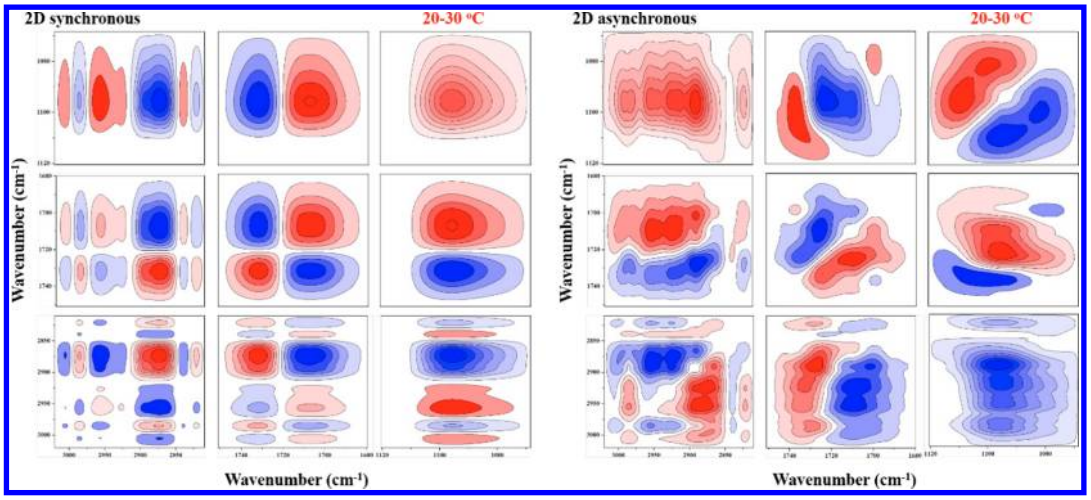


**Figure 9.** 2D synchronous and asynchronous spectra of P($MEO_2MA$-*co*-$PEGMA_{2080}$) in $D_2O$ (10 wt %) during heating between 20 and 30 °C. Warm colors (red) are defined as positive intensities, while cool colors (blue) as negative ones.

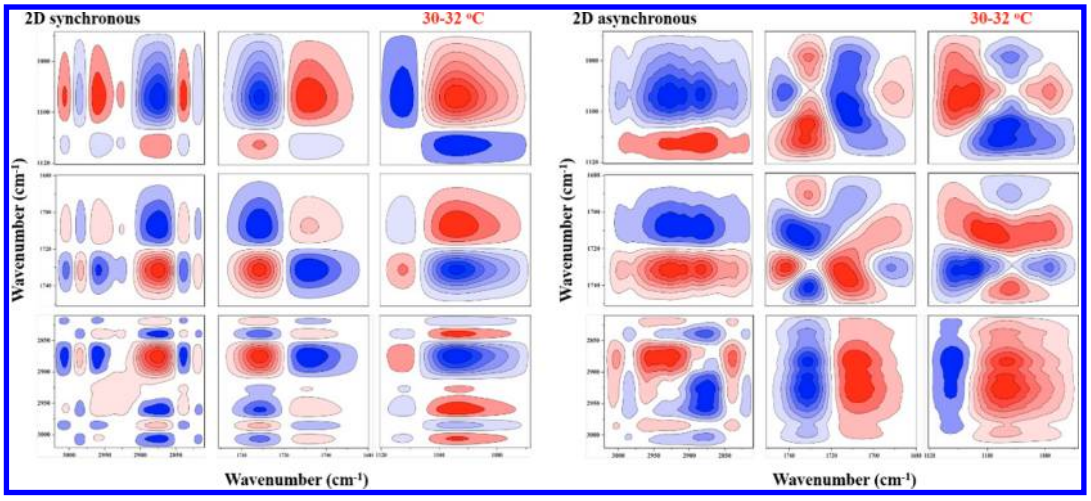


**Figure 10.** 2D synchronous and asynchronous spectra of P($MEO_2MA$-*co*-$PEGMA_{2080}$) in $D_2O$ (10 wt %) during heating between 30 and 32 °C. Warm colors (red) are defined as positive intensities, while cool colors (blue) as negative ones.

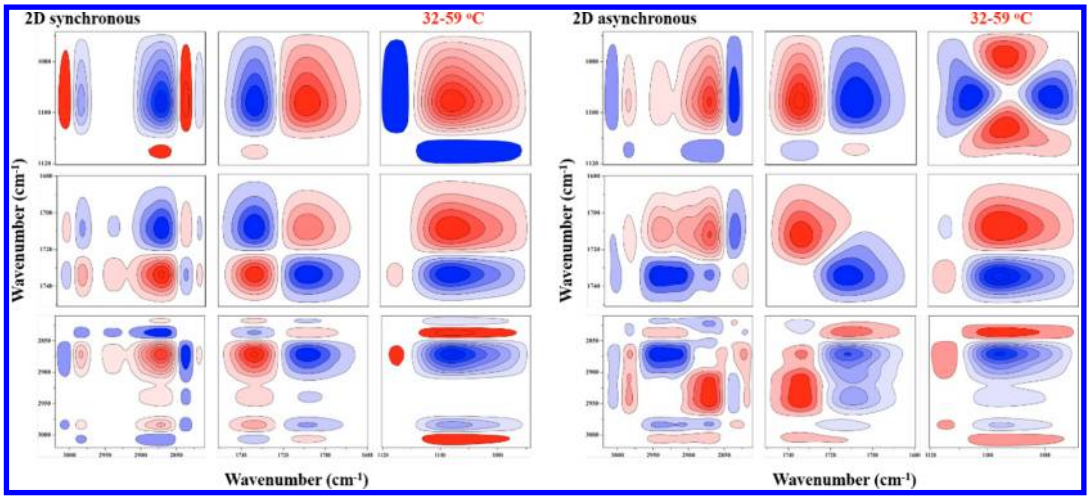


**Figure 11.** 2D synchronous and asynchronous spectra of P($MEO_2MA$-*co*-$PEGMA_{2080}$) in $D_2O$ (10 wt %) during heating between 32 and 59 °C. Warm colors (red) are defined as positive intensities, while cool colors (blue) as negative ones.

**3.3. Two-Dimensional Correlation Analysis.** 2Dcos is a mathematical method originally proposed by Noda[36,37] and it has been considerably applied to interpret spectroscopic intensity fluctuations under different types of external perturbations (e.g., temperature, pressure, concentration, time, electromagnetic) ever since.[38] By spreading the original spectra


dx.doi.org/10.1021/ma500774g | *Macromolecules* 2014, 47, 4728−4737

along a second dimension, features not readily visible in conventional analysis can be sorted out and hence, spectral resolution enhancement can be achieved. In addition, 2Dcos can be applied to deduce the specific sequence order of different chemical groups under a certain physical or chemical variable.

However, as the phase transition process of P($MEO_2MA$-*co*-$PEGMA_{2080}$) is relatively complex, it might be not suitable to apply all the FTIR spectra in heating between 20 and 59 °C to generate the 2Dcos spectra. According to our previous 1D analysis, the heating process was divided into three subregions: 20−30, 30−32, and 32−59 °C. FTIR spectra in these three regions were individually applied to generate the 2Dcos spectra and the obtained synchronous and the asynchronous spectra are shown in Figure 9, 10, and 11.

2D synchronous spectra provide information on simultaneous changes between two wavenumbers. For instance, the bands relating to C═O have negative cross-peaks, indicating that they display opposite sensitivities to temperature perturbation, that is, one decrease with the other increasing during heating determined from raw spectra. 2D asynchronous spectra can significantly enhance the resolution of the original spectra. In Figures 9, 10 and 11, many subtle bands such as the bands at 1735 $cm^{-1}$ attributed from $\nu$(C═O)(dehydrated) as well as four C−O−C splitting bands at 1110, 1105, 1093, and 1078 $cm^{-1}$ that cannot be easily observed in the 1D analysis have been identified. These additionally observed bands relating to subtle group conformations could provide more detailed information and significantly assist in figuring out the mechanism of the complex phase transition process. For clarity, all the bands found in asynchronous spectra and their corresponding assignments have been presented in Table 1.

**Table 1. Tentative Band Assignments of P($MEO_2MA$-*co*-$PEGMA_{2080}$) in $D_2O$ According to 2DCOS Results[23,39−41]**

| wavenumber ($cm^{-1}$) | tentative assignments |
|---|---|
| 3000 | $\nu_{as}(CH_3)(-OCH_3)$ (hydrated) |
| 2989, 2983 | $\nu_{as}(CH_3)(-OCH_3)$ (dehydrated) |
| 2954 | $\nu_{as}(CH_2)(-OCH_2CH_2O-)$ (hydrated) |
| 2942 | $\nu_{as}(CH_2)(-OCH_2CH_2O-)$ (dehydrated) |
| 2925 | $\nu_{as}(CH_2)$ (backbone) |
| 2871 | $\nu_s(CH_3)(-OCH_3)$ |
| 2836 | $\nu_s(CH_2)(-OCH_2CH_2O-)$ (hydrated) |
| 2821 | $\nu_s(CH_2)(-OCH_2CH_2O-)$ (dehydrated) |
| 1735 | $\nu$(C═O) (dehydrated) |
| 1726 | $\nu$(C═O) (semidehydrated) |
| 1710 | $\nu$(C═O) (hydrated) |
| 1695 | $\nu$(C═O) (hydrated) long chain |
| 1110, 1105 | $\nu$(−C−O−C−) (dehydrated) |
| 1093, 1078 | $\nu$(−C−O−C−) (hydrated) |

As both comonomers of P($MEO_2MA$-*co*-$PEGMA_{2080}$) are of the same kind (i.e., both contain a PEG segment and a methacrylate moiety),[7,23] we regarded the random copolymer as a homopolymer and did not distinguish them in detail from IR spectral assignments.

Except for enhancing spectral resolution, 2Dcos can also provide useful information on the specific sequence order of the chemical groups taking place under external perturbation. The judging rule can be summarized as Noda's role-that is, if cross-peaks ($\nu_1$, $\nu_2$, assume $\nu_1 > \nu_2$) in the synchronous and asynchronous maps have the same symbol, both positive or both negative, then we can conclude that change at $\nu_1$ occurs prior to that at $\nu_2$ with the perturbation; whereas if cross-peaks ($\nu_1$, $\nu_2$) in the synchronous and asynchronous maps have different symbols, one positive and the other one negative, then we can infer that peak $\nu_2$ varies prior to peak $\nu_1$.[42]

*3.3.1. Temperature Region I: 20−30 °C.* Temperature region I between 20 and 30 °C was first analyzed in the heating process. The determination details of sequential orders have been presented in the Supporting Information, and here the final sequence order in temperature region I is described as(→ means earlier than or prior to): 2954 $cm^{-1}$ → 3000 $cm^{-1}$ → 1110 $cm^{-1}$ → 1726 $cm^{-1}$ → 1093 $cm^{-1}$ → 2836 $cm^{-1}$ → 1078 $cm^{-1}$ → 2871 $cm^{-1}$→ 1710 $cm^{-1}$ → 2821 $cm^{-1}$ → 2989 $cm^{-1}$, or $\nu_{as}(CH_2)(-OCH_2CH_2O-)$ (hydrated) → $\nu_{as}(CH_3)$-$(-OCH_3)$ (hydrated) → $\nu$(C−O−C) (dehydrated) → $\nu$(C═O) (semidehydrated) → $\nu$(C−O−C) (hydrated) → $\nu_s(CH_2)$-$(-OCH_2CH_2O-)$ (hydrated) → $\nu_s(CH_3)(-OCH_3)$ → $\nu$(C═O) (hydrated) → $\nu_s(CH_2)(-OCH_2CH_2O-)$ (dehydrated)→ $\nu_{as}(CH_3)(-OCH_3)$ (dehydrated).

Without considering the differences in stretching modes of the chemical groups, the specific order can be summarized as follows: $-OCH_2CH_2O-$ → $-OCH_3$→ C−O−C → C═O. This sequence reveals that, in temperature region I, the dehydration of hydrophilic side chain takes place before the dehydration of carbonyl groups and backbones, and the conformation changes of C−H groups in side chains have a more significant effect on the phase transition than the abruption of hydrogen bonds between ether oxygen groups and water molecules.[23] As the C−H group is more hydrophobic compared to ether oxygen group, the resultant structure would still contain some water molecules due to ether oxygen group, which was later defined as clusters. Thus, the driving force of this phase transition process of P($MEO_2MA$-*co*-$PEGMA_{2080}$) should be the dehydration of side chains, especially the short side chains belonging to $MEO_2MA$, which possess low LCST. The phase transition process is similar to that ofP($MEO_2MA$-*co*-$OEGMA_{475}$) and the conformation changes of oxyethylene side chain groups along with the dehydration process play a key role in the formation of clusters as the starting point. The subsequent phase transition behavior of P($MEO_2MA$-*co*-$PEGMA_{2080}$) changed due to the introduction of $PEGMA_{2080}$, which would be discussed later.

On the other hand, if we carefully analyze the asynchronous spectra of P($MEO_2MA$-*co*-$PEGMA_{2080}$), only one obvious cross-peak at (1726,1710 $cm^{-1}$) could be observed. This result is in good accordance with our curve fitting results, i.e. the phase transition could be roughly identified as the transition between 1710 and 1726 $cm^{-1}$ attributed to hydrated C═O and semidehydrated C═O, respectively. The appearance of the band at 1726 $cm^{-1}$, a semidehydrated C═O, implied the formation of a loose hydrophobic structure still containing some water at 30 °C, which was defined as clusters.

Additionally, if we only consider C−H stretching modes of side chains, an interesting sequence can be found that the asymmetric stretching vibration has an earlier response than the symmetric stretching vibration, no matter for methyl or methylene groups.[23] The direction of asymmetric stretching vibration is parallel to the chain axis while that of symmetric stretching vibration is vertical to the chain axis.[43] Therefore, the oxyethylene side chains collapse first to get close to the hydrophobic backbones and then distort to expose hydrophilic ether oxygen groups to the "outer shell" of polymer chains during this heating process. The resulting structure from this


dx.doi.org/10.1021/ma500774g | Macromolecules 2014, 47, 4728−4737

process would be a loose hydrophobic structure, which was defined as clusters.

*3.3.2. Temperature Region II: 30–32 °C.* Temperature region II between 30 and 32 °C was analyzed because the integral area of C═O and transmittance in turbidity measurement showed a reverse change. First, to visually compare Figure 9 and Figure 10, we can find that most synchronous spectra have the same color while most asynchronous spectra have the opposite color, implying the two transition process are similar but opposite. Another interesting phenomenon is the autocorrelation peak at 1710 $cm^{-1}$in the synchronous spectra during heating between 30 and 32 °C is relatively weak compared to that between 20 and 30 °C. It is concluded that most C═O have completed the transition from hydrated state to semidehydrated state at 30 °C, adjustment of different types of semidehydrated C═O would be the main transition, as discussed below. As a result, the autocorrelation peak at 1710 $cm^{-1}$ would be relatively weak.

By using the same method utilized in temperature region I, the determination details of sequential orders in temperature region II have been presented in the Supporting Information, and the final sequence order in temperature region II is described as 2821 $cm^{-1}$ → 2983 $cm^{-1}$ → 2871 $cm^{-1}$ → 1105 $cm^{-1}$ → 1078 $cm^{-1}$ → 1695 $cm^{-1}$ → 1735 $cm^{-1}$ → 1093 $cm^{-1}$ → 1726 $cm^{-1}$ → 1710 $cm^{-1}$ → 1110 $cm^{-1}$ → 3000 $cm^{-1}$ → 2836 $cm^{-1}$ → 2954 $cm^{-1}$, or $\nu_s(CH_2)(-OCH_2CH_2O-)$ (dehydrated) → $\nu_{as}(CH_3)(-OCH_3)$ (dehydrated) → $\nu_s(CH_3)$-$(-OCH_3)$ → $\nu(-C-O-C-)$ (dehydrated) → $\nu(-C-O-C-)$ (hydrated) → $\nu(C═O)$ (hydrated) long chain → $\nu(C═O)$ (dehydrated) → $\nu(C═O)$ (semidehydrated) → $\nu(C═O)$ (hydrated) → $\nu_{as}(CH_3)(-OCH_3)$ (hydrated) → $\nu_s(CH_2)$-$(-OCH_2CH_2O-)$ (hydrated) → $\nu_{as}(CH_2)(-OCH_2CH_2O-)$ (hydrated).

Without considering the differences in stretching modes of the chemical groups, the specific order can be also displayed as follows: $-OCH_2CH_2O-$ → $-OCH_3$→ C−O−C → C═O. This sequence is the same as that in temperature region I. During this process, the hydrophilic side chain takes place before hydrophobic carbonyl groups and backbones, and the conformation changes of C−H groups in side chains have a more significant effect on the phase transition than the abruption of hydrogen bonds between ether oxygen groups and water molecules.[23] Thus, the driving force of this phase transition process of P($MEO_2MA$-*co*-$PEGMA_{2080}$) should also be hydration changes of side chains. However, even the response order of temperature region II is the same as that of temperature region I through roughly analysis. Different details could be obtained after further analysis, as discussed below.

To carefully analyze the C═O region of asynchronous spectra of P($MEO_2MA$-*co*-$PEGMA_{2080}$), two new bands at 1735 and 1695 $cm^{-1}$ occurred, which could be attributed to dehydrated C═O and hydrated C═O with long PEG chain, respectively. The band at 1735 $cm^{-1}$ represents the appearance of totally dehydrated C═O, implying some semidehydrated C═O form in 30 °C undergoing further dehydration. We attributed the band at 1695 $cm^{-1}$ to hydrated C═O with long PEG chain because long PEG chain would attract more water around the polymer chain and stronger hydrogen interaction between C═O and water would be formed, which would result in lower frequency. The appearance of band at 1735 $cm^{-1}$ represent the long PEG chain, which belonged to $PEGMA_{2080}$, beginning to take part in the phase transition. The result C═O belonging to $PEGMA_{2080}$, would be more hydrophobic and collapsed with the dehydrated $MEO_2MA$ chain to form a hydrophobic core. Different types of C═O would have a redistribution in this process. However, the long PEG chain of $PEGMA_{2080,}$ which possess good interaction with water molecule, would exist as the shell of the micelle. The structure of the polymer would change from clusters at 30 °C to micelle at 32 °C. The formation of micelle would result in the redistribution of different types of C═O in the solution, and thus result in the rise of the integral area of C═O. According to previous study, the conformation adjustment upon further heating was due to the difference of different segments in the block copolymer chain.[27−31] In our system, no obvious different segments could be found in random copolymer, the conformation adjustment are mainly due to the amphiphilic property of $PEGMA_{2080}$.

Different result could be obtained in the C−H stretching modes of side chains analysis. Symmetric stretching vibration of $CH_2(-OCH_2CH_2O-)$ had an earlier response than the asymmetric stretching vibration, while the asymmetric stretching vibration of $CH_3(-OCH_3)$ had an earlier response than the symmetric stretching vibration. Thus, it is concluded that the oxyethylene side chains distort to expose hydrophilic ether oxygen groups to form shell of the micelle first and then collapse to get close to the hydrophobic backbones. This response sequence is different from that in 20 and 30 °C, which could also account for the change of the integral area of CH.

*3.3.3. Temperature Region III: 32–59 °C.* Temperature region III between 32 and 59 °C was analyzed utilizing the same method. To visually compare Figure 11 with Figure 9 and Figure 10, we can find that even some similarities exited in the synchronous spectra, the asynchronous spectra is totally different, implying a different transition process.

The determination details of sequential orders in temperature region III have been presented in the Supporting Information, and here the final sequence order in temperature region III is described as 1093 $cm^{-1}$ → 1078 $cm^{-1}$→ 1105 $cm^{-1}$ → 2821 $cm^{-1}$ → 1710 $cm^{-1}$ → 3000 $cm^{-1}$ → 2983 $cm^{-1}$ → 1735 $cm^{-1}$ → 2871 $cm^{-1}$ → 2836 $cm^{-1}$ → 2942 $cm^{-1}$, or $\nu$(C−O−C) (hydrated) → $\nu$(−C−O-C−) (dehydrated) → $\nu_s(CH_2)$-$(-OCH_2CH_2O-)$ (dehydrated) → $\nu(C═O)$(hydrated) → $\nu_{as}(CH_3)(-OCH_3)$ (hydrated) → $\nu_{as}(CH_3)(-OCH_3)$ (dehydrated) → $\nu(C═O)$ (dehydrated) → $\nu_s(CH_3)(-OCH_3)$ → $\nu_s(CH_2)(-OCH_2CH_2O-)$ (hydrated) → $\nu_{as}(CH_2)$-$(-OCH_2CH_2O-)$ (dehydrated)

To neglect the differences in stretching modes of the chemical groups, the specific order can be also summarized as follows: C−O−C → $-OCH_2CH_2O-$ → C═O→ $-OCH_3$. During this process, the change of hydrophilic side chain takes place before that of carbonyl groups and backbones and thus the driving force of this phase transition process of P($MEO_2MA$-*co*-$PEGMA_{2080}$) should also be hydration change of side chains, which is the same to that in temperature region I. However, the abruption of hydrogen bonds between ether oxygen groups and water molecules have a more significant effect on the phase transition than the conformation changes of C−H groups in side chains in this process, which is opposite to that in temperature region I. According to this result, it could be concluded that the ether oxygen groups would break hydrogen bond with water to form dense aggregates, which is different from clusters formed at 30 °C.

Herein, in the C═O region of asynchronous spectra of P($MEO_2MA$-*co*-$PEGMA_{2080}$), only one cross-peak at (1735 $cm^{-1}$, 1710 $cm^{-1}$) could be observed. The phase transition


dx.doi.org/10.1021/ma500774g | *Macromolecules* 2014, 47, 4728−4737

Scheme 2. Schematic Illustration of the Dynamic Mechanism of the Phase Transition of P($MEO_2MA$-*co*-$PEGMA_{2080}$) during Heating

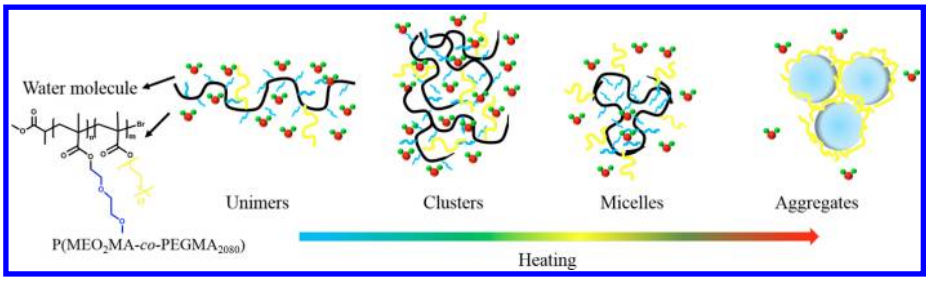


could be roughly identified as the transition from 1710 to 1735 $cm^{-1}$ attributed to hydrated C═O and dehydrated C═O, respectively. The band at 1735 $cm^{-1}$ represent totally dehydrated C═O, implying the formation of a dense hydrophobic structure without water at 59 °C, which was defined as aggregates.

Same result could be obtained in the C−H stretching modes of side chains analysis in temperature region II. Symmetric stretching vibration of $CH_2$(−$OCH_2CH_2O$−) had an earlier response than the corresponding asymmetric stretching vibration, while the asymmetric stretching vibration of $CH_3$(−$OCH_3$) had an earlier response than the corresponding symmetric stretching vibration. Thus, it is concluded that the oxyethylene side chains in the shell of the micelle formed at 32 °C broke hydrogen interaction with water first and then collapse to get close to the hydrophobic backbones to form dense aggregates.

In general, the change of hydrophilic side chain takes place before that of carbonyl groups and backbones during the whole process and thus the driving force of this phase transition process of P($MEO_2MA$-*co*-$PEGMA_{2080}$) should be hydration changes of side chains. During temperature region I, the conformation changes of C−H groups in side chains have a more significant effect on the phase transition than the abruption of hydrogen bonds between ether oxygen groups and water molecules. The bands at 1726 $cm^{-1}$ also provided strong support for this structure and the oxyethylene side chains collapse first to get close to the hydrophobic backbones and then distort to expose hydrophilic ether oxygen groups to the "outer shell" of polymer chains to form loose hydrophobic clusters structure at around 30 °C. Upon further heating, $PEGMA_{2080}$ with long PEG chain helps to form core and shell of a micelle due to its amphiphilic property between $MEO_2MA$ and water. The oxyethylene side chains distort to expose hydrophilic ether oxygen groups to form shell of the micelle first and then collapse to get close to the hydrophobic backbones to form micelle structure at around 32 °C. In temperature region III, the abruption of hydrogen bonds between ether oxygen groups and water molecules have a more significant effect on the phase transition than the conformation changes of C−H groups in side chains to form dense aggregates. The bands at 1735 $cm^{-1}$also provided strong support for this structure and the oxyethylene side chains in the shell of the micelle broke hydrogen interaction with water first and then collapse to get close to the hydrophobic backbones to form dense aggregates at 59 °C. In short, during the whole phase transition process, P($MEO_2MA$-*co*-$PEGMA_{2080}$) chains successively experience "unimers−clusters−micelles− aggregates" four consecutive conformation changes, as shown in Scheme 2.

## 4. CONCLUSIONS

In this paper, we employed turbidity and FTIR measurements, in combination with curve fitting and 2Dcos methods, to investigate the thermally induced phase transition behavior of the P($MEO_2MA$-*co*-$PEGMA_{2080}$). Direct evidence of different structure in different temperatures are given utilizing FT-IR analysis for the first time. While a two-stage aggregation phenomenon could be observed in the turbidity measurements, detailed FT-IR analysis further find that the two-stage aggregation could be divided into three processes. By utilizing curve fitting, the phase transition process could be attributed to the complex transition between hydrated C═O, semidehydrated C═O and dehydrated C═O. Finally, 2Dcos was employed to elucidate the thermally dynamic hydration mechanism of P($MEO_2MA$-*co*-$PEGMA_{2080}$) chains, which successively experience "unimers−clusters−micelles−aggregates" four consecutive conformation changes during the apparent two-stage aggregation process. The hydrophilic side chain takes place before carbonyl groups and backbones during the whole process and the driving force of this phase transition process of P($MEO_2MA$-*co*-$PEGMA_{2080}$) should be hydration changes of side chains. Additionally, the $PEGMA_{2080}$, with long PEG side chain, plays an important role in the structural adjustment process of P($MEO_2MA$-*co*-$PEGMA_{2080}$).

## ■ ASSOCIATED CONTENT

### Supporting Information

TGPC measurements ofP($MEO_2MA$-*co*-$PEGMA_{2080}$) (Figure S1), $^1H$ NMR measurements ofP($MEO_2MA$-*co*-$PEGMA_{2080}$) (Figure S2), and operation details of the sequence order determination during different temperature regions during heating process. This material is available free of charge via the Internet at http://pubs.acs.org.

## ■ AUTHOR INFORMATION

### Corresponding Author

*(P.W.) E-mail: peiyiwu@fudan.edu.cn.

### Notes

The authors declare no competing financial interest.

## ■ ACKNOWLEDGMENTS

We are very grateful for the financial support of the National Natural Science Foundation of China (NSFC) (No. 21274030).

## ■ REFERENCES

(1) Qiu, Y.; Park, K. *Adv. Drug Delivery Rev.* **2012**, *64*, 49.
(2) Bajpai, A. K.; Bajpai, J.; Saini, R.; Gupta, R. *Polym. Rev.* **2011**, *51*, 53.
(3) Yu, L.; Ding, J. D. *Chem. Soc. Rev.* **2008**, *37*, 1473.

(4) Schild, H. G. *Prog. Polym. Sci.* **1992**, *17*, 163.
(5) Wei, H.; Cheng, S. X.; Zhang, X. Z.; Zhuo, R. X. *Prog. Polym. Sci.* **2009**, *34*, 893.
(6) Akdemir, O.; Badi, N.; Pfeifer, S.; Zarafshani, Z.; Laschewsky, A.; Wischerhoff, E.; Lutz, J. F. In *Controlled/Living Radical Polymerization: Progress in ATRP*; Matyjasewski, K., Ed.; American Chemical Society: Washington, DC, 2009; Vol. *1023*, p 189.
(7) Lutz, J. F. *J. Polym. Sci., Polym. Chem.* **2008**, *46*, 3459.
(8) Lutz, J. F.; Akdemir, O.; Hoth, A. *J. Am. Chem. Soc.* **2006**, *128*, 13046.
(9) Hu, Z. B.; Cai, T.; Chi, C. L. *Soft Matter* **2010**, *6*, 2115.
(10) Lutz, J. F.; Hoth, A. *Macromolecules* **2006**, *39*, 893.
(11) Weber, C.; Hoogenboom, R.; Schubert, U. S. *Prog. Polym. Sci.* **2012**, *37*, 686.
(12) Lutz, J. F. *Adv. Mater.* **2011**, *23*, 2237.
(13) Wischerhoff, E.; Uhlig, K.; Lankenau, A.; Borner, H. G.; Laschewsky, A.; Duschl, C.; Lutz, J. F. *Angew. Chem., Int. Ed.* **2008**, *47*, 5666.
(14) Qiao, Z. Y.; Du, F. S.; Zhang, R.; Liang, D. H.; Li, Z. C. *Macromolecules* **2010**, *43*, 6485.
(15) Jonas, A. M.; Hu, Z. J.; Glinel, K.; Huck, W. T. S. *Nano Lett.* **2008**, *8*, 3819.
(16) Gibson, M. I.; Paripovic, D.; Klok, H. A. *Adv. Mater.* **2010**, *22*, 4721.
(17) Yoon, J. A.; Gayathri, C.; Gil, R. R.; Kowalewski, T.; Matyjaszewski, K. *Macromolecules* **2010**, *43*, 4791.
(18) Ryu, J. H.; Chacko, R. T.; Jiwpanich, S.; Bickerton, S.; Babu, R. P.; Thayumanavan, S. *J. Am. Chem. Soc.* **2010**, *132*, 17227.
(19) Dong, H. C.; Matyjaszewski, K. *Macromolecules* **2010**, *43*, 4623.
(20) Becer, C. R.; Hahn, S.; Fijten, M. W. M.; Thijs, H. M. L.; Hoogenboom, R.; Schubert, U. S. *J. Polym. Sci., Polym. Chem.* **2008**, *46*, 7138.
(21) Miasnikova, A.; Laschewsky, A. *J. Polym. Sci., Polym. Chem.* **2012**, *50*, 3313.
(22) Ishizone, T.; Seki, A.; Hagiwara, M.; Han, S.; Yokoyama, H.; Oyane, A.; Deffieux, A.; Carlotti, S. *Macromolecules* **2008**, *41*, 2963.
(23) Sun, S. T.; Wu, P. Y. *Macromolecules* **2013**, *46*, 236.
(24) Ieong, N. S.; Hasan, M.; Phillips, D. J.; Saaka, Y.; O'Reilly, R. K.; Gibson, M. I. *Polym. Chem.* **2012**, *3*, 794.
(25) Yao, Z. L.; Tam, K. C. *Polymer* **2012**, *53*, 3446.
(26) Peng, B. L.; Grishkewich, N.; Yao, Z. L.; Han, X.; Liu, H. L.; Tam, K. C. *ACS Macro Lett.* **2012**, *1*, 632.
(27) Trinh, L. T. T.; Lambermont-Thijs, H. M. L.; Schubert, U. S.; Hoogenboom, R.; Kjoniksen, A. L. *Macromolecules* **2012**, *45*, 4337.
(28) Zhang, Z. X.; Liu, K. L.; Li, J. *Macromolecules* **2011**, *44*, 1182.
(29) Xie, D. H.; Ye, X. D.; Ding, Y. W.; Zhang, G. Z.; Zhao, N.; Wu, K.; Cao, Y.; Zhu, X. X. *Macromolecules* **2009**, *42*, 2715.
(30) Yamamoto, S.; Pietrasik, J.; Matyjaszewski, K. *Macromolecules* **2007**, *40*, 9348.
(31) Hua, F. J.; Jiang, X. G.; Zhao, B. *Macromolecules* **2006**, *39*, 3476.
(32) Lutz, J. F.; Weichenhan, K.; Akdemir, O.; Hoth, A. *Macromolecules* **2007**, *40*, 2503.
(33) Cho, E. C.; Lee, J.; Cho, K. *Macromolecules* **2003**, *36*, 9929.
(34) Schmidt, P.; Dybal, J.; Trchova, M. *Vib. Spectrosc.* **2006**, *42*, 278.
(35) Skrovanek, D. J.; Howe, S. E.; Painter, P. C.; Coleman, M. M. *Macromolecules* **1985**, *18*, 1676.
(36) Noda, I. *Appl. Spectrosc.* **1993**, *47*, 1329.
(37) Noda, I.; Dowrey, A. E.; Marcott, C.; Story, G. M.; Ozaki, Y. *Appl. Spectrosc.* **2000**, *54*, 236A.
(38) Noda, I. *J. Mol. Struct.* **2008**, *883*, 2.
(39) Sun, B. J.; Lai, H. J.; Wu, P. Y. *J. Phys. Chem. B* **2011**, *115*, 1335.
(40) Maeda, Y.; Kubota, T.; Yamauchi, H. *Langmuir* **2007**, *23*, 11259.
(41) Maeda, Y.; Yamauchi, H.; Kubota, T. *Langmuir* **2009**, *25*, 479.
(42) Noda, I. *Appl. Spectrosc.* **2000**, *54*, 994.
(43) Sun, S. T.; Tang, H.; Wu, P. Y.; Wan, X. H. *Phys. Chem. Chem. Phys.* **2009**, *11*, 9861.